Journal of Applied Fluid Mechanics, Vol. 16, No. 6, pp. 1269-1280, 2023.
Available online at www.jafmonline.net, ISSN 1735-3572, EISSN 1735-3645.
https://doi.org/10.47176/jafm.16.06.1587

Numerical Study on End Wall Synthetic Jet to Improve Performance and Stability Margin of a High-speed Subsonic Axial Compressor Rotor

G. Wang[1†], W. Chu[2] and W. Liu[2]

[1] *School of Aeronautics and Astronautics, Guilin University of Aerospace Technology, Guilin, Guangxi, 541004, China*
[2] *School of Power and Energy, Northwestern Polytechnical University, Xi'an, Shanxi, 710129, China*

†*Corresponding Author Email: wangguang@mail.nwpu.edu.cn*

(Received October 10, 2022; accepted February 26, 2023)

ABSTRACT

Synthetic jet has been confirmed as a novel flow control technology. However, the existing application research on synthetic jet in axial flow compressor is still confined to cascade or low-speed axial flow compressors, and rarely high-speed axial flow compressor. The effects of three vital parameters (i.e., the action position, frequency, peak velocity) on the aerodynamic performance and stability margin are systematically studied, with a high-speed compressor rotor as the object of numerical simulation. An optimal excitation position is determined, corresponding to the core position of the compressor top blockage, as indicated by the results, which increases the stability margin and efficiency of the compressor by 13.2% and 1.15% respectively. The excitation frequency has a threshold ranging from 300Hz to 600Hz. Only when the frequency of synthetic jet exceeds this threshold can it suppress the tip leakage flow. Besides, the jet peak velocity may not have a threshold. However, the higher the peak velocity, the greater the mixing loss between the jet and the mainstream of the compressor rotor will be, thus limiting the further increase of the compressor efficiency.

Keywords: Compressor; End wall; Synthetic jet; Performance improvement; Numerical simulation.

NOMENCLATURE

M	mass flow rate	a	inlet measurement sections
γ	loss	b	outlet measurement sections
V	velocity	κ	adiabatic index
t	time	Ca	length of axial chord(mm)
$V(t)$	velocity of synthetic jet	T	period of synthetic jet
$Vmax$	peak velocity of synthetic jet	IN	compressor inlet passage
F	frequency	HUB	compressor hub
Φ	initial phase	TIP	compressor tip
π	total pressure ratio	OUT	compressor outlet passage
E	power	PAS	compressor passage
ρ	density	μ_{eff}	comprehensive viscosity coefficient
A	area	SM	stable margin
η	efficiency	SW	solid wall
P^*	total pressure	ns	neat stall
T^*	total temperature	sj	synthetic jet
V_n	normal velocity	L	location

1. INTRODUCTION

The research on aero-engine has been committed to achieving excellent performance and wide stability margin (Saito *et al.* 2019). Experimental measurement and numerical simulation methods have made great progress as science and technology have been leaping forward. Researchers have gained a deeper insights into axial compressors' internal flow and instability mechanism, and they have developed a wide variety of flow control methods, some of which have been applied to engineering practice. However, the conventional flow control

methods have some defects. For instance, casing treatment improves the stability margin of the compressor at the cost of significantly sacrificing its efficiency (Zhang *et al.* 2019). Although end wall profiling (Kiran and Anish 2017) and vortex generator (Hergt *et al.* 2012) can enhance the performance under off design conditions, they often lead to the reduced performance of design points. Boundary layer suction (Zhang *et al.* 2018) and steady/unsteady jet (Wang *et al.* 2014) require complex external pipelines. Plasma excitation is capable of enhancing the stability margin and aerodynamic performance of the compressor only at low speeds (Vo 2007). Synthetic jet, a novel type of active flow control technology, shows the advantages of fast response, good effect, no complex pipeline, and low energy consumption (Smith and Glezer 1998; Amitay and Glezer 2002). It refers to a flow control technology with great application prospects, and it is a direction of axial compressors that is worthy of in-depth research.

For compressor cascade, existing research has suggested that flow separation and total pressure loss can be reduced under reasonable excitation parameters (Culley *et al.* 2004; Matejka *et al.* 2008; Zander *et al.* 2011; De Giorgi *et al.* 2012). However, if a flow control technology is to be applied to the field of aero-engine, a systematical study of this technology should be conducted first in the compressor with a more complex flow field. Existing research results have suggested that the research object of synthetic jet in compressors is primarily cascade, and rare research objects are axial compressors. For instance, NASA Glenn Research Center has experimentally studied the synthetic jet on the suction surface of stator blades on an axial compressor, whereas its design speed is only 980 rpm (Braunscheidel *et al.* 2008). For another example, Benini et al. carried out a numerical study on the arrangement of synthetic jet on the blades of NASA rotor 37, whereas they only studied individual working conditions (e.g., design point and near stall point) (Benini *et al.* 2011; Biollo *et al.* 2012). Accordingly, the existing research on applying synthetic jet in the axial compressor lacks comprehensiveness and systematicness.

The main aims of this study are presented as follows:

(a) To verify the effectiveness of end wall synthetic jet to expand the stability margin and enhance the aerodynamic performance of high-speed axial flow compressor.

(b) To examine the influence law of three vital parameters of synthetic jet.

(c) To reveal the influence mechanism of the end wall synthetic jet on the compressor through detailed flow and loss analysis.

2. RESEARCH OBJECTS AND METHODS

2.1 Research Object

The research object of this study is an isolated rotor of an axial compressor test bench with a design speed of 15200rpm. The test bench comprises DC motor, booster, compressor rotor, exhaust section and measuring equipment (Wu *et al.* 2014). Air enters radially and exits axially. The geometric data of the rotor include the rotor blade of 30, the blade tip chord length of 30mm, the aspect ratio of 1.925, the blade tip installation angle of 37˚10′, the blade root installation angle of 59˚50′, as well as the blade tip clearance of 0.3mm. The main design indicators of the studied compressor rotor in this paper include the mass flow rate of 5.6kg/s, the total pressure ratio of 1.249, and the adiabatic efficiency of 0.905.

2.2 Numerical Simulation Method

The computational domain from the radial inlet to 6 times the chord length of the blade tip downstream of the compressor outlet is built, and the computational domain grid was divided using NUMECA IGG/AutoGrid 5. The calculation domain is divided into two sections. As depicted in Fig. 1, the static domain is from the radial inlet to the front of the rotor, and the rest is the rotating domain. The mesh size of the first layer is set to 5×10^{-6}m. The rotor blade channel adopts O4H grid topology, and 205 grids are set around the blade surface. To improve the simulation accuracy, the butterfly grid topology is adopted for the tip clearance. After grid independence verification, 960000 grids are employed for single channel calculation (Fig. 2).

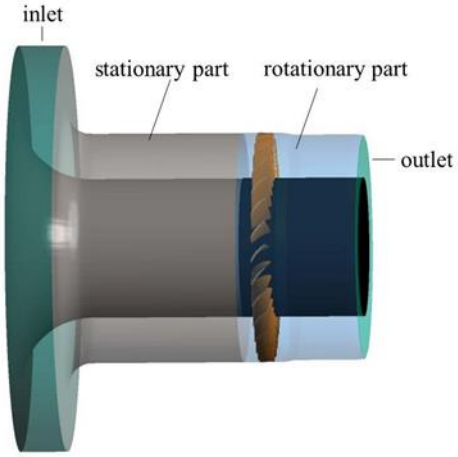

Fig. 1. Structure of compressor rotor.

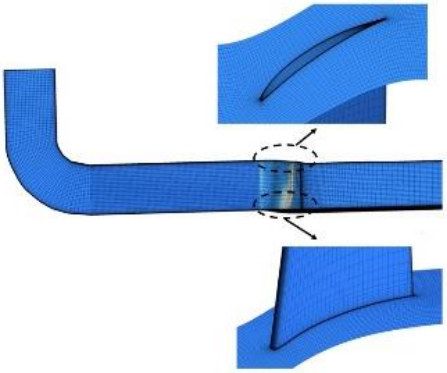

Fig. 2. Computational domain grid and local amplification.

ANSYS CFX software is employed for numerical calculation at 8130 rpm and 10765 rpm to compare the numerical results with the experimental results. To be specific, the turbulence model is k-omega, and the convection term is discretized in the second-order upwind. The inlet boundary conditions of the simulated compressor rotor are total pressure and total temperature. Furthermore, the outlet is the average static pressure, and the solid walls are specified with adiabatic and nonslip state.

Figure 3 presents the total performance obtained by experimental measurement (Lu *et al.* 2007) and numerical calculation. It can be seen that they fit well, whereas there are also some errors. The possible reason for this result is the assumption of ideal gas and the turbulence model selection in numerical calculation. However, the trend of these parameters is consistent, and the distribution of outlet total pressure ratio given in Fig. 4 is consistent with the experimental measurement.

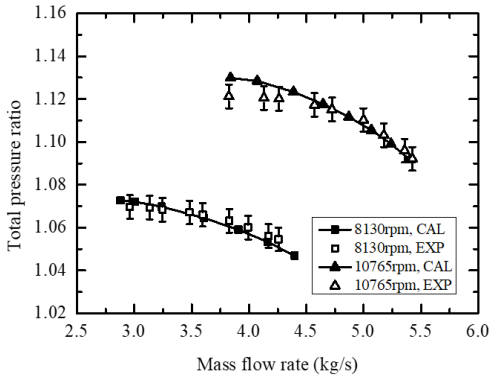

(a) Total pressure ratio

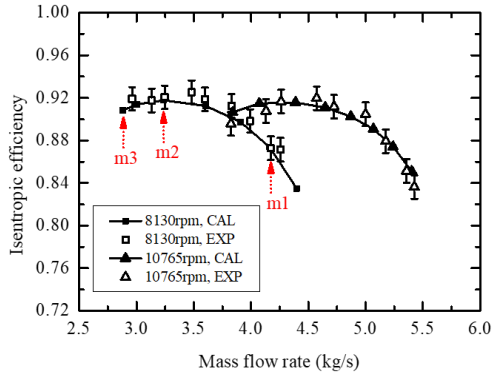

(b) Isentropic efficiency

Fig. 3. Total performance obtained from experimental measurement and numerical calculation.

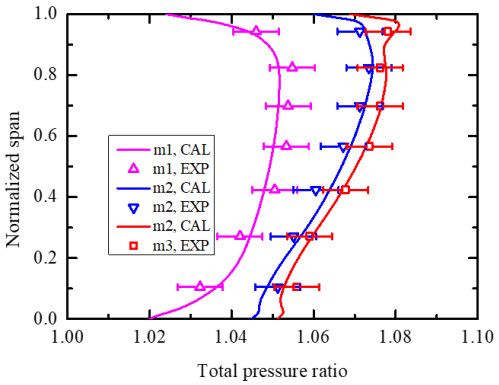

Fig. 4. Comparison of predicted and experimental radial total pressure distributions.

2.3 Internal Flow Analysis

The instability process analysis and synthetic jet excitation of the compressor rotor are simulated at 8130rpm. Figure 5 presents the relative Ma at 99% radial span of rotor blade. The flow at the tip of the compressor rotor is good under high flow conditions. A low-speed zone appears near the trailing edge of the pressure surface at the peak efficiency point. Although there is a certain blockage to the flow at the tip of the rotor, it is not enough to block the whole blade tip due to the small range. As the compressor rotor throttles to the near stall point, the blade tip blockage area increases significantly due to the increased outlet back pressure, such that the compressor exhibits instability.

A question is raised about why the compressor has more serious tip blockage with the increase of throttling. Figure 6 presents the radial velocity contour of the blade suction surface. Moreover, the hub wall is colored by static pressure to characterize the throttling degree. With the throttling of the compressor, the radial velocity of the flow close to the wall of the trailing edge increases significantly compared with the high flow condition. The increase of the radial velocity will enable some low-speed airflow originally gathered in the corner of the rotor to flow to the blade tip. On that basis, the diffuser capacity of the compressor will be improved, and more serious tip blockage will be caused. Thus, diffuser capacity and tip load are a pair of contradictions for the compressor.

The flow loss is quantitatively described by dividing the loss by region (Li *et al.* 2014). Since the fluid

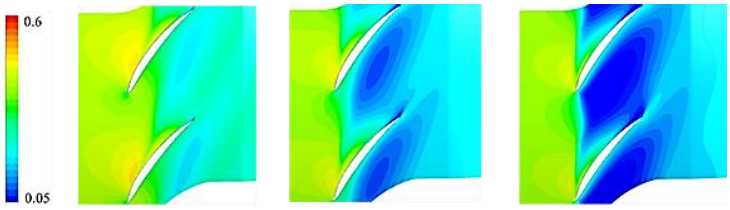

(a) m1 (b) m2 (c) m3

Fig. 5. Relative Mach contour of 99% span.

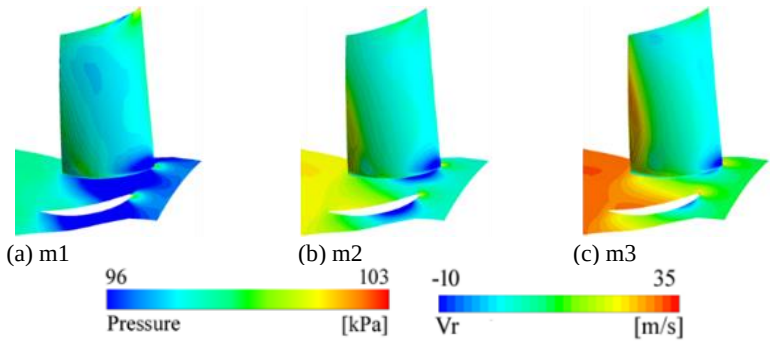

(a) m1 (b) m2 (c) m3

Fig. 6. Radial velocity contour of suction surface and static pressure contour of hub.

velocity shear will produce dissipation, and the dissipation function is the only term in the fluid equation that can convert mechanical energy into heat energy, therefore, the loss amount of a divided region could be calculated by three-dimensional integration of the dissipation function. Subsequently, the loss source can be obtained by dimensionless inlet dynamic pressure. This method overcomes the deficiency of total pressure loss coefficient and expresses the local loss.

The loss of an area is defined as below:

$$\gamma_{source} = \frac{\Delta p^*_{source}}{p^*_{in} - p_{in}} = \frac{\iiint_{region} \Phi \mathrm{d}x\mathrm{d}y\mathrm{d}z}{(p^* - p)_{in} \iint_{in} V_n \mathrm{d}A} \quad (1)$$

The tensor form of the dissipation function $\boldsymbol{\Phi}$ is shown as below:

$$\Phi(x,y,z) = \frac{\mu_{eff}}{2}\left(\frac{\partial u_i}{\partial x_j} + \frac{\partial u_j}{\partial x_i}\right)^2 + \frac{2}{3}\mu_{eff}\left(\frac{\partial u_i}{\partial x_i}\right)^2 \quad (2)$$

As depicted in Fig. 7, the loss source of the compressor rotor can be divided into five parts.

① Loss of inlet: γ_{IN}. Its volume integration range is as follows: axially from the inlet measured section to the leading edge of the rotor blade; radial from 2% span to the casing.

② Loss of hub: γ_{HUB}. Its volume integration range is as follows: axially from the inlet measured section to the outlet measured section; radial from the hub to 2% span.

③ Loss of tip leakage and separation: γ_{TIP}. Its volume integration range is as follows: axially from the leading edge to the trailing edge; radial from 85% span to the casing.

④ Loss of outlet: γ_{OUT}. Its volume integration range is as follows: axially from the trailing edge to the outlet measured section; radial from 2% span to the casing.

⑤ Loss of passage: γ_{PAS}. Its volume integration range is as follows: other areas.

It should be pointed out that the tip leakage flow of this studied compressor rotor is mainly distributed above 90% span, so the radial boundary between tip leakage loss and passage loss is 85%.

Figure 8 presents the proportion of each area loss to the total loss of the compressor. The proportion of

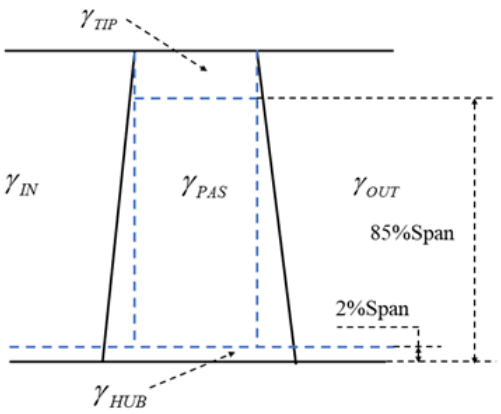

Fig. 7. Loss division.

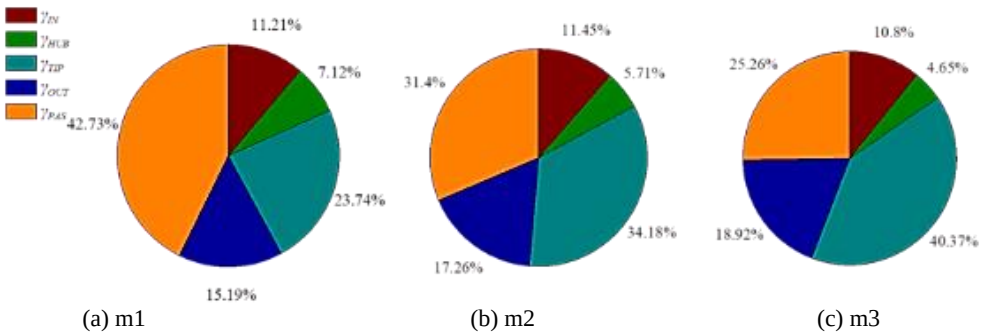

(a) m1 (b) m2 (c) m3

Fig. 8. Proportion of each loss in total loss.

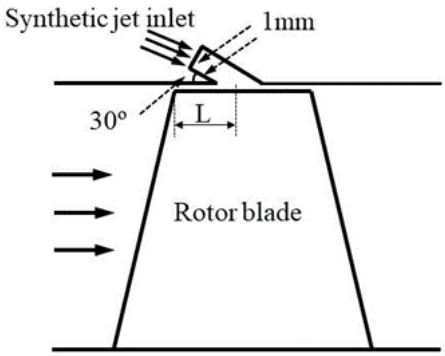

Fig. 9. Synthetic jet calculation model.

γ_{IN}, γ_{HUB} and γ_{OUT} in the total loss changes little, while γ_{TIP} and γ_{PAS} change significantly. With the throttling of compressor rotor, the proportion of γ_{PAS} tends to decrease, whereas the proportion of γ_{TIP} increases significantly, reaching over 40%. As revealed by the change of loss in the respective region, the loss of the compressor rotor is primarily concentrated in the blade tip and passage. Thus, taking reasonable flow control measures at the blade tip is expected to reduce the loss of the compressor rotor.

3. SIMULATION MODEL OF END WALL SYNTHETIC JET

As depicted in Fig. 9, the flow in the slot and the compressor channel are considered a single connected domain in the simulation of this paper. The groove is arranged on the outside of the casing to simulate the slit structure of the actuator. The top of the groove is the velocity inlet boundary condition of the synthetic jet during the simulation, the velocity is expressed in Eq. (3), and the walls on both sides of the slot are set as adiabatic and non-slip conditions, respectively.

$$V(t) = V_{\max} \sin(2\pi ft + \varphi) \tag{3}$$

The groove is fully covered in the circumferential direction to simplify the model and eliminate the effect of the initial phase of jet velocity. Accordingly, the initial phase does not affect the results, and is set to 0 during the simulation. When the unsteady calculation of synthetic jet is simulated, the time term is discretized by the second-order backward Euler scheme, the physical time step is set to 1/20 of a synthetic jet cycle, and 10 virtual time steps are set under the respective physical time step.

4. RESULT ANALYSIS

In this study, the effect of three vital parameters is primarily studied (i.e., the action position, frequency, peak velocity). The calculation is also conducted at 8130rpm.

The improvement of comprehensive stability margin (Yan and Chu 2021) is defined:

$$\Delta SM = \left(\frac{m_{SW.ns}}{m_{sj.ns}} \times \frac{\pi_{sj.ns}}{\pi_{SW.ns}} - 1\right) \times 100\% \tag{4}$$

Where m denotes the flow, the subscripts SW and sj represent the prototype and the compressor excited by end wall synthetic jet, respectively; the subscript ns expresses near stall condition.

It is worth pointing out that the power required when the synthetic jet is injected into the compressor should be determined using the method proposed by Jin (Jin *et al.* 2005):

$$E = \frac{1}{2}\rho \cdot A \cdot (0.26 V_{\max}^3) \tag{5}$$

Where E is the power, ρ is the density, and A is the inlet area of the synthetic jet. Thus, the calculation of compressor efficiency is revised as below:

$$\eta = \frac{(p_b^* / p_a^*)^{(\kappa-1)/\kappa} - 1}{T_b^* / T_a^* - 1 + E / m / (\kappa / (\kappa - 1)) / R / T_a^*} \tag{6}$$

The variation of efficiency is defined as below:

$$\Delta\eta = \frac{\eta_{sj} - \eta_{SW}}{\eta_{SW}} \times 100\% \tag{7}$$

4.1 Effect of Excitation Position

Six excitation places (L/Ca) studied in this study are listed as follows: L1=-16.67%, L2=5.56%, L3=22.22%, L4=44.44%, L5=66.67% and L6=94.44%. Moreover, frequency and peak velocity of synthetic jet remain constant as follows: f =600Hz, V_{max}=50m/s. The settings of calculation parameters and other parameters of the jet remain unchanged.

Figure 10 and 11 presents the effects of synthetic jet arranged at six places of casing on the total pressure ratio, isentropic efficiency, and stall margin of the subsonic axial compressor rotor. As revealed by the influence on the total pressure ratio, the end wall synthetic jet has little influence under the condition of large flow, but from the flow of peak efficiency point to the that of near stall point, except for the first two places, the end wall synthetic jet at the other four excitation places improves the total pressure ratio of the simulated compressor rotor. When the compressor excited by different places is at the near stall flow rate of the unexcited compressor, the end wall synthetic jet at L3 increases the total pressure ratio by 0.14%. The first two places slightly affect the efficiency in the whole flow range, and the end wall synthetic jet at the other four places significantly increases the efficiency. At the flow rate of m point, the end wall synthetic jet at L3, L4, and L5 increases the efficiency of the compressor by 1.15%, 1.4%, and 1.35%, whereas the peak efficiency increases by 0.34%, 0.67%, and 0.83%, respectively. As indicated by the effect on the comprehensive stability margin of the compressor, the variation of the comprehensive stability margin is positive, and it tends to first increase and then decrease. This result reveals that the synthetic jet at six positions increases the comprehensive stability margin of the compressor to varying degrees, whereas the influence results at different positions are different.

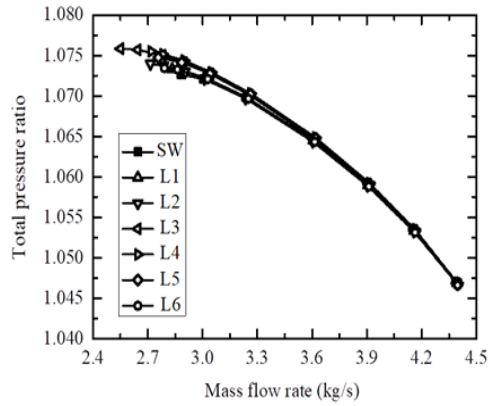

(a) Total pressure ratio

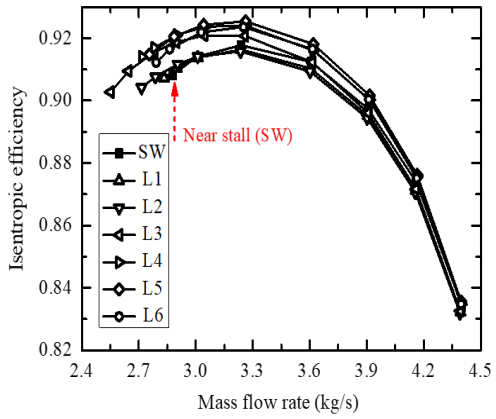

(b) Isentropic efficiency

Fig. 10. Total performance of compressor excited by synthetic jet at different positions.

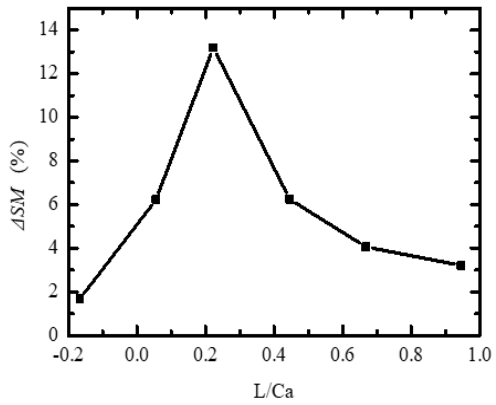

Fig. 11. Correlation between of comprehensive stability margin and excitation position

The increase amplitude of excitation at L3 position is the largest, reaching 13.2%, and the increase amplitude at L1 position is the smallest, only 1.68%. Given the improvement magnitude of aerodynamic performance and stability change of the simulated rotor, the optimal action place of excitation is L3 and the worst action place is L1.

The near stall flow point in Figure 10 (b) is selected to compare and analyze the internal flow field of the compressor excited by the end wall synthetic jet at different places, so as to reveal the excited mechanism.

Figure 12 presents the change of relative Mach number contour of 99% span in one cycle under the excitation (T1 to T8 represent typical moments in a synthetic jet cycle). As depicted in the figure, when the synthetic jet position is 2mm before the leading edge (L1 position), the top blockage degree of the rotor is slightly reduced at the blowing stage, whereas it is restored at the suction stage. In general, the blockage change of the rotor top is not significant. The reason is that the blowing and suction effects are far away from the blocked low-energy air mass, and the excitation effect cannot be effectively played. As the position of synthetic jet moves backward, it is closer to the low-speed flow area, thus resulting in the rotor tip blockage. Both blowing and suction are capable of blowing or absorbing low-energy fluid and reduce the degree of blade tip blockage. The figure also indicates the blowing and suction effect of synthetic jet on low-speed flow at rotor tip achieves the optimal effect at L3 position, because L3 position is roughly in the core area of blade tip blockage of the unexcited compressor. At the blowing stage, high-speed jet generated by the excitation blows the top blocked low-energy air mass downstream. Accordingly, the figure reveals that the blocked core area moves downstream. Moreover, due to the phase lag characteristic of the compressor rotor response caused by the end wall excitation, this trend continues until T7 at the suction stage. So the blockage at the blade tip of the compressor is alleviated, and the stability margin of the rotor is effectively enlarged. Nevertheless, as the excitation position continues to move backward, the effect of blowing and suction begins to weaken. When the synthetic jet is in L4 place, the blade tip blockage area is divided into two parts with nearly the same area under the action of the jet at the blowing stage. Since the excitation position is in the core position of the blade tip blockage of the prototype compressor, the blockage of the divided upstream part is still more serious than that of the downstream part. The

blockage of the upstream part becomes more significant as the position of the synthetic jet continues to move back to L5. When the position of the synthetic jet moves back to the trailing edge L6 of the rotor, it can hardly blow and suction the blocked low-energy air flow, and stability margin of the compressor cannot be well improved. Therefore, it can be concluded that for the subsonic axial flow compressor simulated in this paper, the best excitation position is the core position of the tip blockage.

Figure 13 presents the magnitude of various losses of the prototype compressor and the changes of various losses of end wall synthetic jet excitation at different positions in a cycle. γ_{TIP} changes most significantly, followed by γ_{OUT}, and a slight difference is identified in other losses. With the change of the different action position, γ_{TIP} shows a "V" shape change law. Moreover, γ_{TIP} under the excitation of L3 reaches the minimum, which is reduced by 44.13% and 40.5% on average in a synthetic jet cycle respectively.

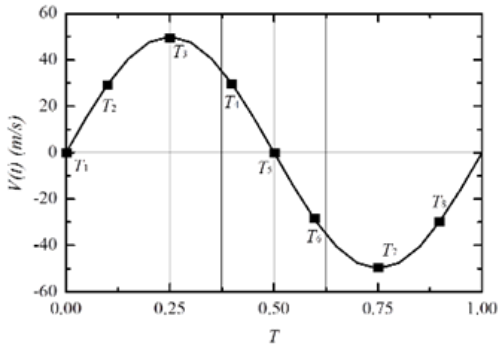

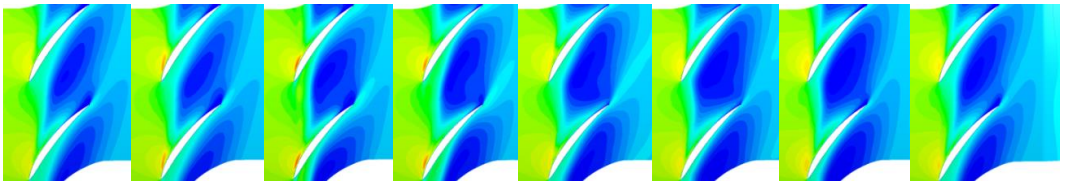

T_1 T_2 T_3 T_4 T_5 T_6 T_7 T_8

(a) L1

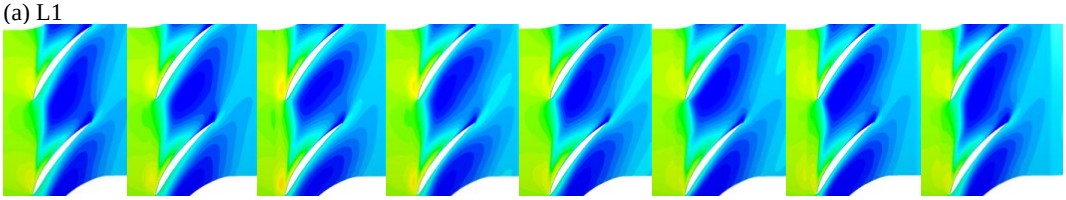

T_1 T_2 T_3 T_4 T_5 T_6 T_7 T_8

(b) L2

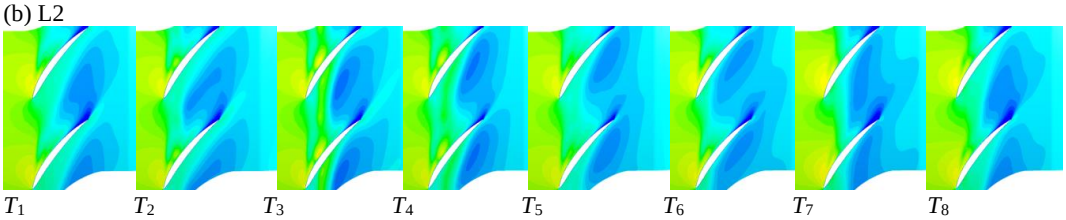

T_1 T_2 T_3 T_4 T_5 T_6 T_7 T_8

(c) L3

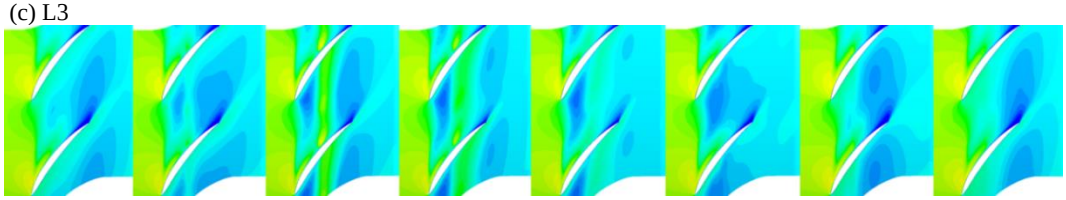

T_1 T_2 T_3 T_4 T_5 T_6 T_7 T_8

(d) L4

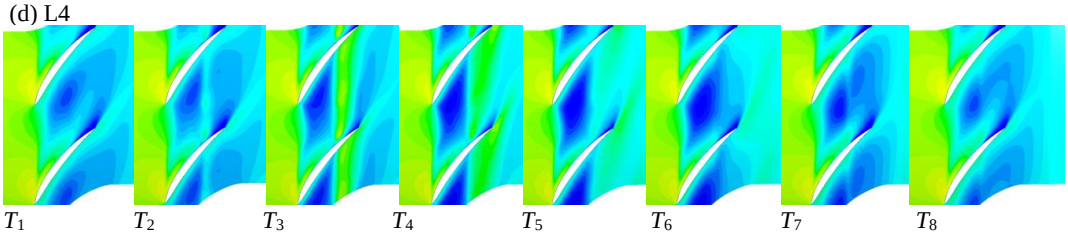

T_1 T_2 T_3 T_4 T_5 T_6 T_7 T_8

(e) L5

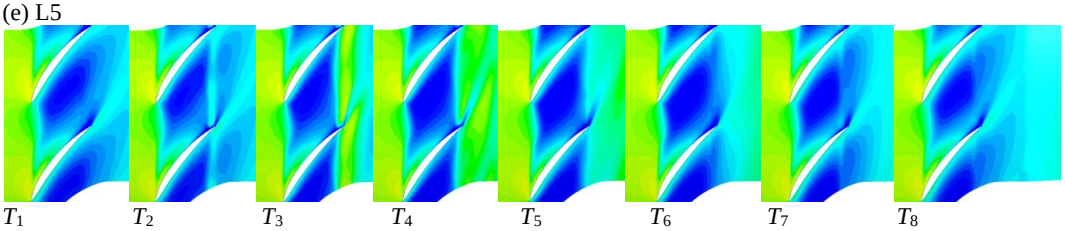

T_1 T_2 T_3 T_4 T_5 T_6 T_7 T_8

(f) L6

Fig. 12. Relative Mach contour of 99% span.

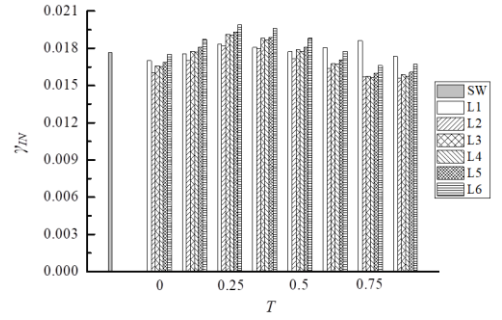

(a) Loss of inlet

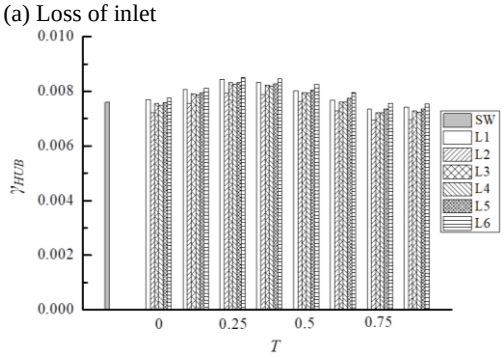

(b) Loss of hub

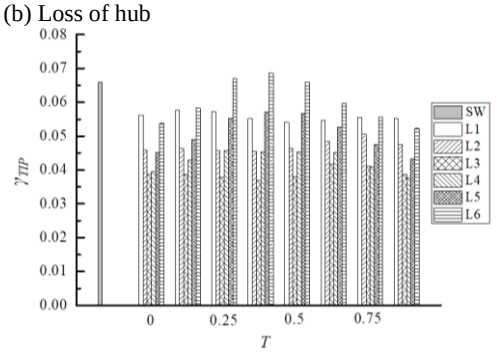

(c) Loss of tip leakage and separation

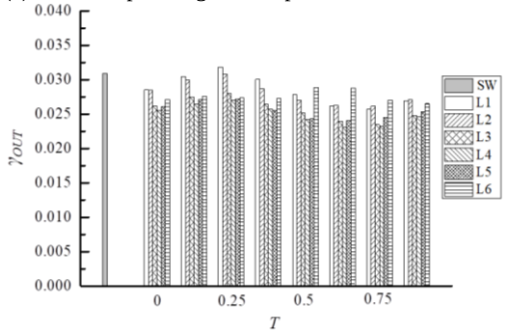

(d) Loss of outlet

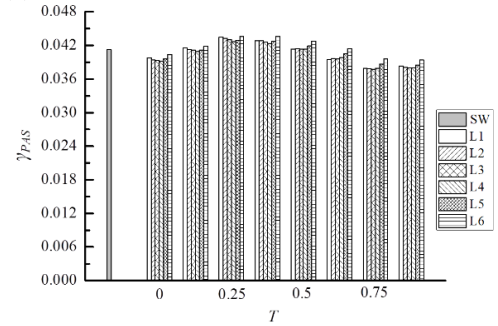

(e) Loss of passage

Fig. 13. Variation of various losses of compressor.

4.2 Effect of Excitation Frequency

Seven frequencies studied are listed as follows: f 1=25Hz, f 2=50Hz, f 3=100Hz, f 4=200Hz, f 5=300Hz, f 6=600Hz, f 7=1200Hz. Moreover, action place and peak velocity of synthetic jet remain constant as follows: L/Ca=L3, V_{max}=50m/s. The settings of calculation parameters and other parameters of the jet remain unchanged.

For clarity, Fig. 14 only shows the excited compressor rotor's performance at three typical frequencies. As depicted in the figure, under the high flow condition, the end wall synthetic jet with different frequencies has similar and slight influence on the performance parameters of the compressor rotor. When the compressor rotor works at the flow rate between the peak efficiency point and the near stall point, the end wall synthetic jet with different frequencies increases its pressure ratio, and the greater the excitation frequency, the stronger the rotor's compression capacity. Nevertheless, little difference is identified in efficiency improvement.

Figure 15 presents the variation of the comprehensive stability margin of the compressor at seven excitation frequencies. As depicted in the figure, the synthetic jet at seven frequencies expands the comprehensive stability margin of the compressor, whereas there is no linear correlation between the change of the comprehensive stability margin and the excitation frequency. Besides, this change is divided into three sections as follows.

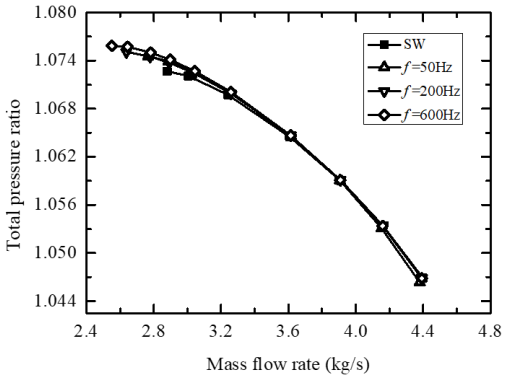

(a) Total pressure ratio

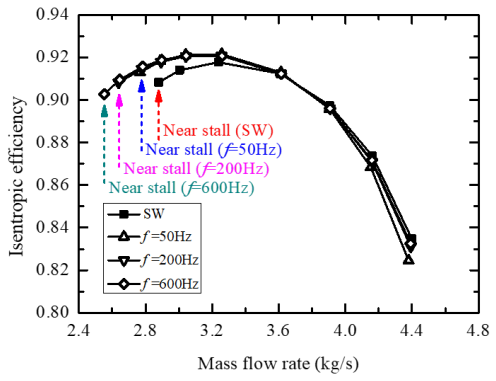

(b) Isentropic efficiency

Fig. 14. Total performance of compressor excited by synthetic jet at three typical frequencies.

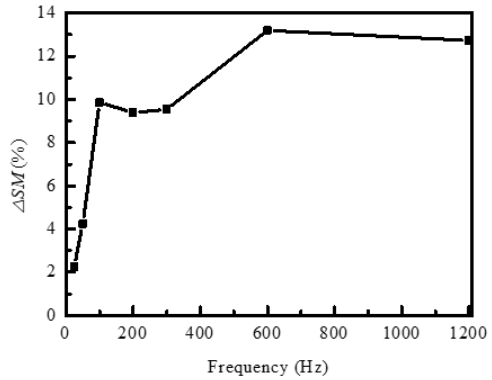

Fig. 15. Variation of comprehensive stability margin of compressor at seven jet frequencies.

Under the low-frequency (25Hz, 50Hz) excitation, the change of the comprehensive stability margin is small though the rotor's performance can be well-promoted; at the low-frequency stage, the comprehensive stability margin shows a linear relationship with jet frequency. When the jet frequency rises to the intermediate frequency (i.e., 100Hz, 200Hz, and 300Hz), the comprehensive stability margin of the compressor increases significantly, reaching 9%-10%, and it remains stable in this frequency range. When the jet frequency increases to a high frequency continuously (i.e., 600Hz and 1200Hz), the comprehensive stability margin of the compressor increases again, reaching 12%-14%. According to the compressor performance and stall margin changes at 7 excitation frequencies studied in this paper, a preliminary conclusion can be drawn as follows: when the excitation is arranged at the optimal place of the end wall of the rotor's casing, the total performance will be more significantly enhanced, and the comprehensive stability margin will be more expanded with the increase of the jet frequency.

From the perspective of working for compressor: when the peak velocity of the synthetic jet is the same, the higher its excitation frequency, the more work it does to the air flow in the compressor rotor per unit time, and the jet momentum will quickly reach and exceed the minimum momentum controlling the flow field at the compressor blade tip in a longer time. In other words, the low-speed clogged area at the compressor blade tip will not be recovered before it is in the next blowing or suction excitation. Accordingly, from this point of view, for the subsonic axial flow compressor in this paper, there may be a threshold value for the excitation frequency of the end wall synthetic jet that can completely "control" the flow field at the compressor tip and keep it under "control". This threshold frequency is between 300Hz and 600Hz.

Figure 16 shows the magnitude of various losses of the prototype compressor and the changes of various losses of end wall excitation at seven frequencies in a cycle. Their jet peak velocity is the same, so, the most significant effect is still γ_{TIP} only when the excitation frequency is different. Under high frequency excitation, the tip leakage loss is greater than that of medium and low frequencies at the time

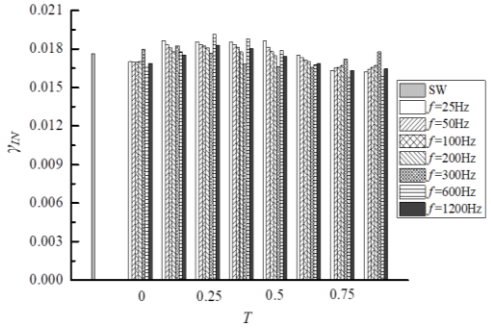

(a) Loss of inlet

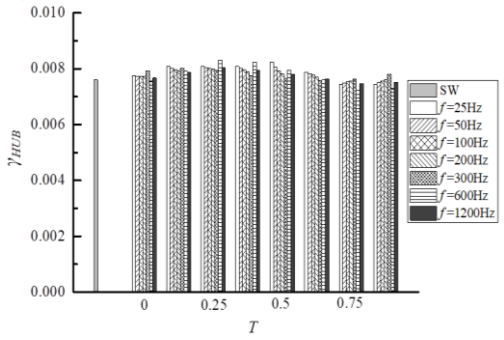

(b) Loss of hub

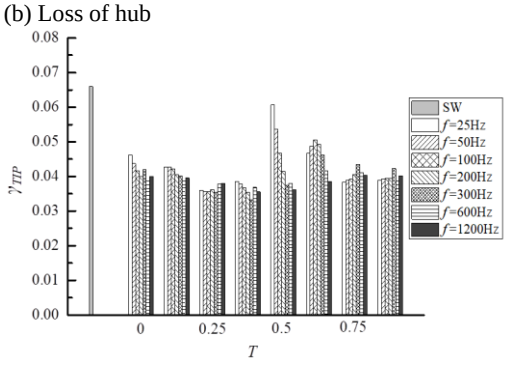

(c) Loss of tip leakage and separation

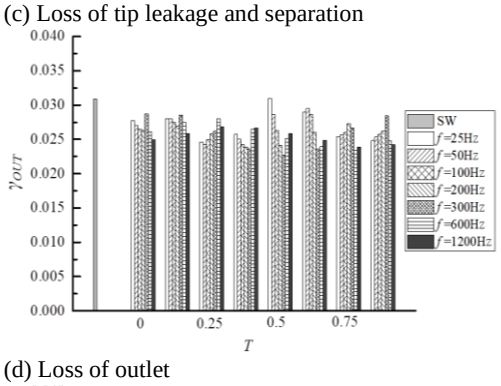

(d) Loss of outlet

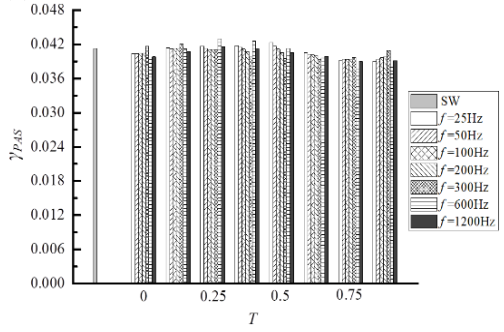

(e) Loss of passage

Fig. 16 Variation of various losses of compressor.

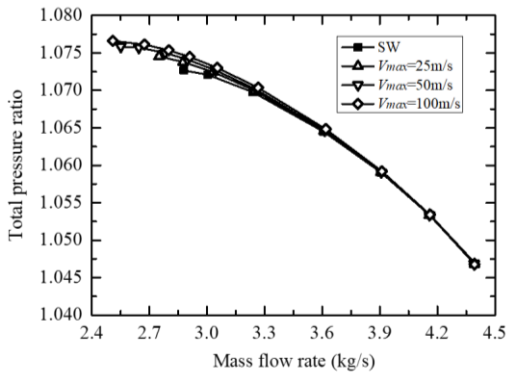

(a) Total pressure ratio

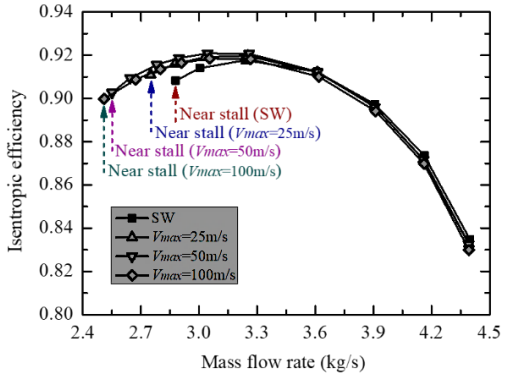

(b) Isentropic efficiency

Fig. 17. Total performance excited by synthetic jet at different peak speeds (f = 600Hz).

4.3 Effect of Jet Peak Velocity

The effects of three jet peak velocities of 25m/s, 50m/s and 100m/s are investigated. Moreover, the action position is still L3, and the frequency is selected as 600Hz greater than the threshold value. The settings of calculation parameters and other parameters of the jet remain unchanged.

Figure 17 shows the performance of the studied high-speed subsonic axial compressor rotor when the synthetic jet is excited by the above three different peak velocities. As depicted in the figure, they all improve the compressor rotor's performance. Comparing the working lines of the compressor rotor under the excitation of three velocity, it can be seen that the near-stall mass flow rate decreases with the increase of jet peak velocity, while the total pressure ratio increases and the isentropic efficiency under medium and low flow conditions increases significantly. However, with the increase of the velocity from 50m/s to 100m/s, the near-stall mass flow rate is reduced, and the isentropic efficiency upgradation is only equivalent to that at 25m/s. It can be obtained by comparison and calculation that under the action of three different jet velocities, the compressor rotor's total pressure ratio increases by 0.106%, 0.136% and 0.169% respectively, and the efficiency increases by 0.85%, 1.15% and 0.91% respectively.

As revealed by the above analysis, the following several views can be obtained: first, for the studied compressor rotor and its performance improvement,

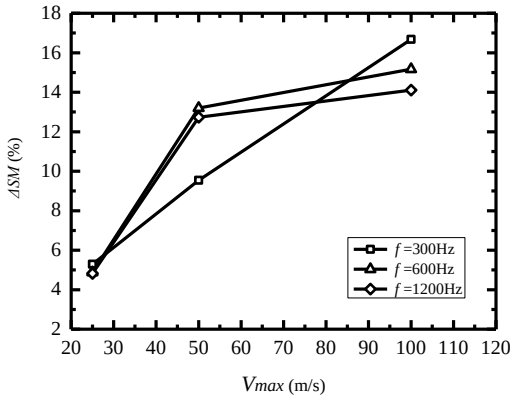

Fig. 18. Correlation between improvement of comprehensive stability margin and jet peak velocity.

there may be no threshold value for jet peak velocity, which is different from the threshold value of excitation frequency. It can significantly produce an effective effect on the compressor rotor, as long as the synthetic jet is at the optimal action position and at the medium or high excitation frequency. Second, there is no positive correlation between the excitation effect and the jet peak velocity. In other words, the greater the jet velocity, the less the improvement of the compressor performance may be. Under the high jet peak velocity excitation, the efficiency is not significantly increased though the compressor still achieves a higher total pressure ratio. The possible reason for this result is that when the jet velocity is too large, the velocity difference between the jet and the low-energy flow at the top of the blade is also large, resulting in more mixing loss during the purging or suction process, which affects the efficiency improvement.

In order to further clarify the coupling effect of jet peak velocity and excitation frequency on the working characteristics of the compressor rotor, we also calculated the influence of the above three jet peak velocities at 300Hz and 1200Hz jet frequencies. Figure 18 presents the correlation between the improvement of comprehensive stability margin of the subsonic axial compressor rotor excited by end wall synthetic jet and the peak jet velocity. At the excitation frequency of 300Hz, the improvement of comprehensive stability margin is nearly linear to the velocity, while at the excitation frequency of 600Hz and 1200Hz, the expansion rule of comprehensive stability margin is similar to influence rule of the velocity. That is, when the jet peak velocity increases, the comprehensive stability margin increases significantly at first, and then slowly. The above results also show that in the study of excitation frequency in the previous section, it is reasonable for us to estimate its threshold higher than 300Hz.

Figure 19 illustrates the variation of various losses inside the compressor rotor. When stimulated by synthetic jet with different jet peak velocities, γ_{TIP} is smaller than that of the unactuated compressor rotor, and γ_{TIP} decreases at other times except 0.25T and 0.375T with the increase of jet peak velocity, which indicates that increasing the excitation velocity is beneficial to restrain the tip leakage flow, reduce the

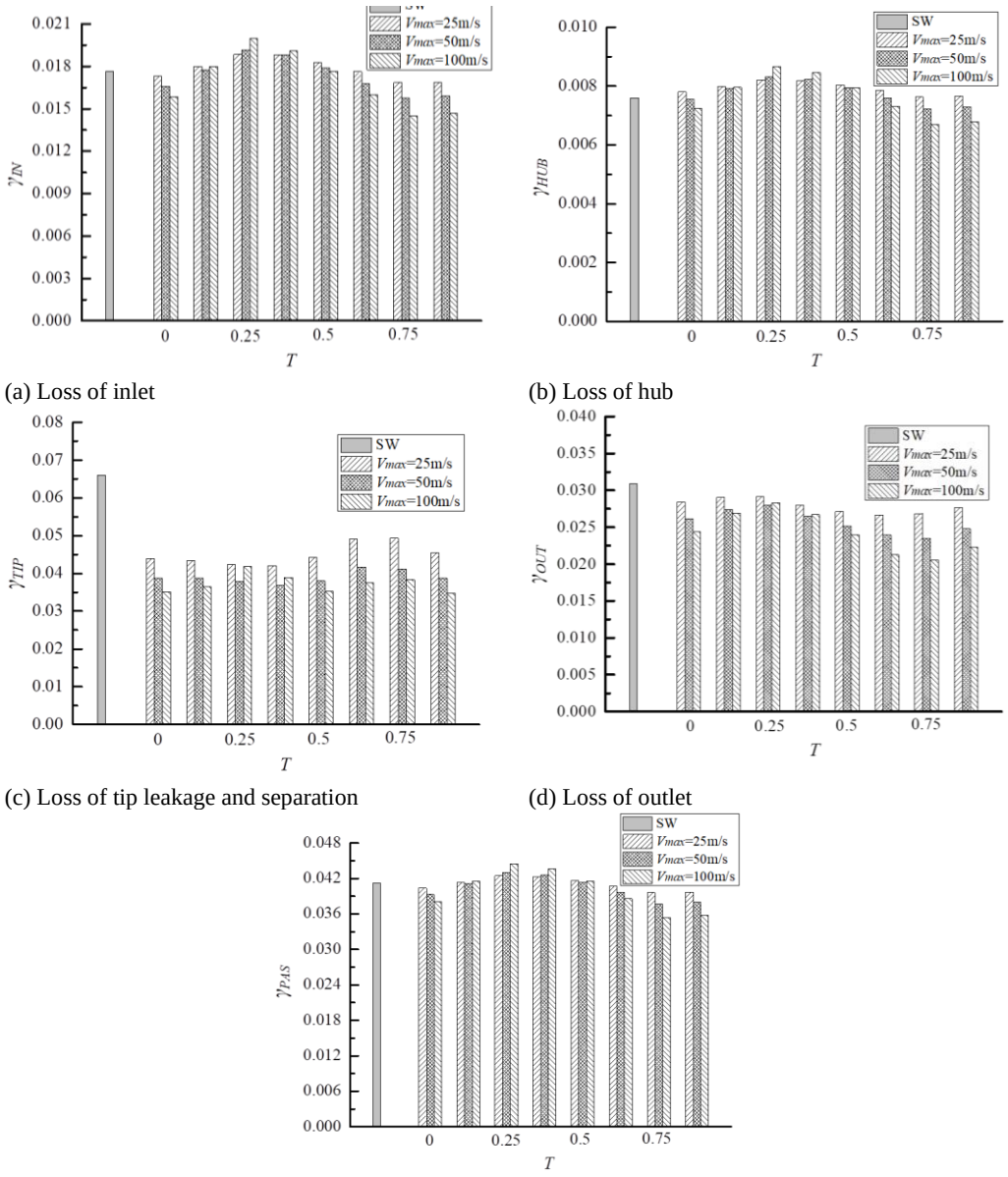

(a) Loss of inlet

(b) Loss of hub

(c) Loss of tip leakage and separation

(d) Loss of outlet

(e) Loss of passage

Fig. 19. Changes of various losses of compressor.

top blockage, and increase the stall margin of the compressor rotor. However, at the too large jet peak velocity (100m/s), the losses at 0.25T and 0.375T exceed that of 50m/s, suggesting that the excessive jet velocity leads to the increased compressor rotor loss and the decreased isentropic efficiency.

5. CONCLUSION

(1) This study confirmed that synthetic jet control technology can also expand the stability margin of high-speed axial compressor and improve its performance.

(2) The synthetic jet has an optimal position on the end wall, which is located above the tip plug core. Under the excitation of that place, the low-energy fluid can be effectively purged or pumped through purging and suction, such that the blockage of the blade tip can be reduced.

(3) Action frequency should have a functional threshold. For the subject and situations studied in this paper, the threshold ranges from 300Hz to 600Hz.

(4) Under the excitation of the best position, due to the increase of mixing loss between mainstream and jet, although the peak velocity increases, the compressor rotor's stability margin and aerodynamic performance will increase slightly.

(5) There are still some deficiencies in this study. in the future, experimental research will be conducted to further verify the conclusions of this study.

ACKNOWLEDGEMENTS

The authors would like to thank the support of National Science and Technology Major Project (No. 2017-II-0005-0018).

REFERENCES

Amitay, M. and A. Glezer (2002). Role of actuation frequency in controlled flow reattachment over a stalled airfoil. *AIAA Journal* 40(2), 209-216.

Benini, E., R. Biollo and R. Ponza (2011). Efficiency enhancement in transonic compressor rotor blades using synthetic jets: a numerical investigation. *Applied Energy* 88(3), 953-962.

Biollo, R., E. Staffieri and E. Benini (2012). On the use of synthetic jets in transonic compressors. In *Turbo Expo: Power for Land, Sea, and Air*, American Society of Mechanical Engineers.

Braunscheidel, E. P., D. E. Culley and K. Zaman (2008). Application of synthetic jets to reduce stator flow separation in a low speed axial compressor. In *46th AIAA Aerospace Sciences Meeting and Exhibit*, 602.

Culley, D. E., M. M. Bright, P. S. Prahst and A. J. Strazisar (2004). Active flow separation control of a stator vane using embedded injection in a multistage compressor experiment. *Journal of Turbomachinery* 126(6), 24-34.

De Giorgi, M. G., S. Traficante, C. De Luca, D. Bello and A. Ficarella (2012). Active flow control techniques on a stator compressor cascade: a comparison between synthetic jet and plasma actuators. In *Turbo Expo: Power for Land, Sea, and Air*, American Society of Mechanical Engineers.

Hergt, A., R. Meyer and K. Engel (2012). Effects of vortex generator application on the performance of a compressor cascade. *Journal of Turbomachinery* 135(2), 021026.

Jin, W. B., K. S. Breuer and C. S. Tan (2005). Active control of tip clearance flow in axial compressors. *Journal of Turbomachinery* 127(2), 352-362.

Kiran, K. N. and S. Anish (2017). An investigation on the effect of pitchwise endwall design in a turbine cascade at different incidence angles. *Aerospace Science and Technology* 71(12), 382-391.

Li, X., W. Chu and Y. Wu (2014). Numerical investigation of inlet boundary layer skew in axial-flow compressor cascade and the corresponding non-axisymmetric end wall profiling. *Proceedings of the Institution of Mechanical Engineers, Part A: Journal of Power and Energy* 228(6), 638-656.

Lu, X., W. Chu and J. Zhu (2007). Numerical investigations of the flow mechanisms in a subsonic compressor rotor with axial skewed slots. *Proceedings of the Institution of Mechanical Engineers, Part A: Journal of Power and Energy* 221(3), 301-313.

Matejka, M., L. Popelka, P. Safarik and J. Nozicka (2008). Influence of active methods of flow control on compressor blade cascade flow. In *Turbo Expo: Power for Land, Sea, and Air*, American Society of Mechanical Engineers.

Saito, S., M. Furukawa, K. Yamada, K. Watanabe and N. Niwa (2019). Mechanisms and quantitative evaluation of flow loss generation in a multi-stage transonic axial compressor. In *Turbo Expo: Power for Land, Sea, and Air*, American Society of Mechanical Engineers.

Smith, B. L. and A. Glezer (1998). The formation and evolution of synthetic jets. *Physics of Fluids* 10(9), 2281-2297.

Vo, H. D. (2007). Suppression of short length-scale rotating stall inception with glow discharge actuation. In *Turbo Expo: Power for Land, Sea, and Air*, American Society of Mechanical Engineers.

Wang, W., W. Chu and H. Zhang (2014). The effect of injector size on compressor performance in a transonic axial compressor with discrete tip injection. *Proceedings of the Institution of Mechanical Engineers, Part A. Journal of Power and Energy* 228(7), 760-771.

Wu, Y., J. Wu, H. Zhang, and W. Chu (2014). Experimental and numerical investigation of flow characteristics near casing in an axial flow compressor rotor at stable and stall inception conditions. *Journal of Fluids Engineering*, 136(11), 111106.

Yan, S. and W. Chu (2021). The improvement of transonic compressor performance by the self-circulating casing treatment. *Proceedings of the Institution of Mechanical Engineers, Part C. Journal of Mechanical Engineering Science*, 235(7), 1165-1176.

Zander, V., M. Hecklau, W. Nitsche, A. Huppertz and M. Swoboda (2011). Active flow control by means of synthetic jets on a highly loaded compressor cascade. *Proceedings of the Institution of Mechanical Engineers, Part A: Journal of Power and Energy* 225(7), 897-906.

Zhang, H., W. Liu, E. Wang, Y. Wu and W. Yao (2019). Mechanism investigation of enhancing the stability of an axial flow rotor by blade angle slots. *Proceedings of the Institution of Mechanical Engineers, Part G: Journal of Aerospace Engineering* 233(13), 4750-4764.

Zhang, P., B. Liu, Y. Yin and J. Yang (2018). Numerical investigation of shroud casing boundary layer suction on a counter-rotating compressor. *Journal of Aeronautics, Astronautics and Aviation* 50(1), 95-112.